World Academy of Science, Engineering and Technology
International Journal of Mechanical and Industrial Engineering
Vol:17, No:3, 2023

An Induction Motor Drive System with Intelligent Supervisory Control for Water Networks Including Storage Tank

O. S. Ebrahim, K. O. Shawky, M. A. Badr, P. K. Jain

***Abstract*—**This paper describes an efficient; low-cost; high-availability; induction motor (IM) drive system with intelligent supervisory control for water distribution networks including storage tank. To increase the operational efficiency and reduce cost, the IM drive system includes main pumping unit and an auxiliary voltage source inverter (VSI) fed unit. The main unit comprises smart star/delta starter, regenerative fluid clutch, switched VAR compensator, and hysteresis liquid-level controller. Three-state energy saving mode (ESM) is defined at no-load and a logic algorithm is developed for best energetic cost reduction. To reduce voltage sag, the supervisory controller operates the switched VAR compensator upon motor starting. To provide smart star/delta starter at low cost, a method based on current sensing is developed for interlocking, malfunction detection, and life–cycles counting and used to synthesize an improved fuzzy logic (FL) based availability assessment scheme. Furthermore, a recurrent neural network (RNN) full state estimator is proposed to provide sensor fault-tolerant algorithm for the feedback control. The auxiliary unit is working at low flow rates and improves the system efficiency and flexibility for distributed generation during islanding mode. Compared with doubly-fed IM, the proposed one ensures 30% working throughput under main motor/pump fault conditions, higher efficiency, and marginal cost difference. This is critically important in case of water networks. Theoretical analysis, computer simulations, cost study, as well as efficiency evaluation, using timely cascaded energy-conservative systems, are performed on IM experimental setup to demonstrate the validity and effectiveness of the proposed drive and control.

***Keywords*—**Artificial Neural Network, ANN, Availability Assessment, Cloud Computing, Energy Saving, Induction Machine, IM, Supervisory Control, Fuzzy Logic, FL, Pumped Storage.

I. Introduction

CLOUD computing and information through Web are now commonly used for modern optimal control and management. Thanks to the advances of Internet of Things (IoT) technology, various social and industrial Web-based applications are now feasible such as; medical diagnosis, information services, smart meters and billing, building and factory management, transportation control, and many other opportunities.

O. S. Ebrahim, Dr., is with the Dept. of Electrical Power and Machines, Faculty of Engineering, Ain Shams University, Egypt (e-mail: osama.shawky@eng.asu.edu.eg).

K. O. Shawky is a student at the Civil Dept., Faculty of Engineering, Ain Shams University, Egypt.

M. A. Badr, Prof., is the Vice President of the Future University, Egypt (e-mail: mabadr@fue.edu.eg).

P. K. Jain, Prof., is the Director of ePOWER Research Center, Queen's University, Ontario, Canada (e-mail: praveen.jain@queensu.ca).

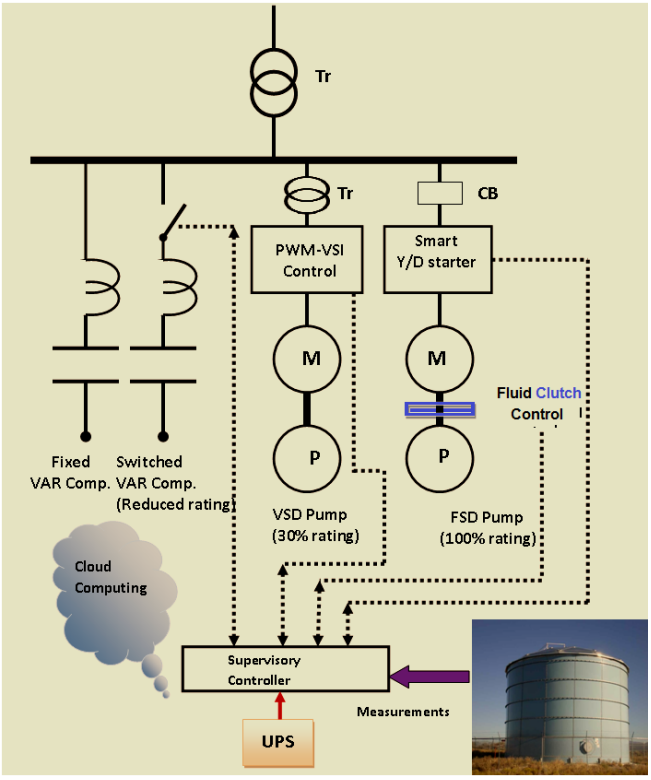

Fig. 1 Blok Diagram of the Proposed Drive System

Fig. 1 shows block diagram of the proposed drive system for a water network that includes storage tank and connected to cloud via internet. The cloud receives massive information from the plant's sensors, controllers, and users. Then, it performs extensive data manipulations and mathematical programming, considering various factors and physical constraints, in order to achieve optimal system management in terms of global impacts such as; reliability, power quality, load demand satisfaction at attractive energetic cost, sustainability, etc. Accordingly, the decisions of a localized-public (i.e., supervisory) control have to be linked, by way of design and objective, to these global impacts [1], [2]. In particular, the operational continuity of water distribution networks has a high priority.

More often than not, optimization of water network's operation requires a hydraulic tank, acting as energy storage or load time-shifter, to achieve cost reduction without violating

the service quality [3], [4]. Hourly and semi-hourly optimization periods are reported to be suitable for pumped hydro-storage in isolated power systems with large penetration of renewable energy [4]. For optimization errors reduction, coordinated operation between hydro-power storage and battery or flywheel energy storage systems has been proposed in [5]. Fig. 2 (a) shows a hydraulic storage tank having input flow rate q_i and load flow q_0 independent of the liquid-level h or head. The governing dynamic equation is given by (1) where, A is the tank cross-section area.

$$\tilde{h}(t) = \frac{1}{A}\int (q_i - q_0)dt \quad (1)$$

The cloud computing generates the head command h^* which satisfies the optimization problem over the specified time period. The supervisory controller achieves this command using on-off control or hysteresis control. Hysteretic controller offers ease of implementation, fast response, and good accuracy against un-modeled dynamics (for instant; tank with variable cross section area) and its adaptive version can resemble the deadbeat control [6]. However, (1) represents a pure integrator that is sensitive to sensor noise and DC offsets [7], [8]. Therefore, online estimation of the liquid-level for fault-tolerant sensor control (i.e., the ability of the controller to operate with satisfactory performance under sensor defects) is problematic especially; q_i and q_o normally are slow time-varying quantities. Despite that there are various adaptive filtering and estimation algorithms in the literature that could be applied to fault-tolerant control of water tank level [9], the RNN based estimator, shown in Fig. 3, has the advantages of inherent redundancy, noise immunity, memory, and learning ability [10]. These features make RNN-based estimation a viable approach for fault-tolerate control of systems with partial state measurements or under sensor failure.

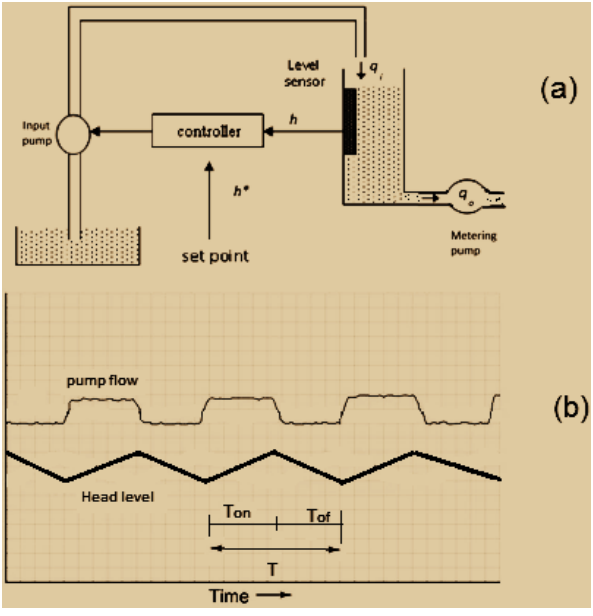

Fig. 2 Storage tank control (a) and plot of input-flow, water-level, and control times (b)

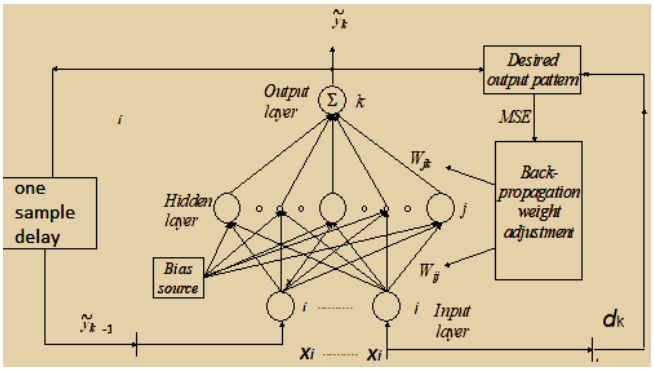

Fig. 3 Three-layer feedforward RNN

In water pumped storage, the energy conservation principle and component's efficiency are the factors, rather than the pump affinity law, for cost and energy savings assessment. Recent recommendations and regulations to replace standard and high efficiency class motors with premium and super-premium ones; make IM a viable choice for the gross cost reduction [11]. The IM driving pumps are cheap, robust and relatively straightforward to operate. However, some precautions have to be taken due to high starting current. It can cause voltage dips and thermal overload which are problematic for the end users of the same power network and for the motor itself. Those problems can be alleviated by choosing suitable motor starting method and appropriate power supply connection [12]. Fig. 1 shows an uninterruptable power supply (UPS) feeding critical (control and protection) system components with electricity in order to make them insensitive to the unavoidable electrical grid disturbances. However, thyristor based soft starter requires expensive fast acting fuses for short circuit protection and malfunction diagnosis [13]. Further, insulated gate bipolar transistor (IGBT) or integrated gate commutated thyristor (IGCT) based pulse width modulated-voltage source inverter (PWM-VSI) is costly to be used as a starter only, [14]-[16], and requires complex connection and synchronization circuits for multi-motor starting system. On the other hand, the star/delta starter is a cheap and effective starting method but; electromechanical contactors suffer from electrical health degradation due to aging [17], [18]. In [18], a sample-data based ANN model is developed to estimate the remaining life-cycles utilizing monitored contact resistance. However, the method is expensive since accurate measurements of the contactor voltage and current are needed. In [15], the inverse model of [18] is proposed to reduce the cost and a software life-cycle counter is used to develop a contactor electrical health assessment algorithm.

Furthermore, implementation of the hysteresis tank level control using motor starter increases the motor thermal stress and adds difficulty to the optimization problem. In such a case, missing the motor thermal information could lead to insulation failure. On the other hand, imposing the maximum permissible number of consecutive start/hr as a constraint in the optimization problem reduces the effectiveness of its solution. This is because the permissible number of

consecutive cold start/hr is different from the permissible number of consecutive hot start/hr [19].

This paper presents an IM drive system for water pumping applications, see Fig. 1, with intelligent; fault-tolerant; supervisory controller. The system includes a fully-rated; fixed-speed; IM pumping unit working at high and medium flow rates using hysteresis liquid-level control and a low-rated; VSI-fed; pumping unit working at low flow rates using efficiency optimized speed control [8], [14]. Since only fraction of the total power is processed through the VSI, the overall system has high operational efficiency, low cost, and flexibility for distributed generation operating in the stand-alone mode with insufficient reserve and high level of uncertainty [20]. Compared with wound-rotor; DFIM having low-rated back-to-back converters [21], the proposed one ensures 30% working throughput under main motor/pump fault conditions. This is critically important in case of water distribution plants. Further, the system has higher efficiency and marginal cost difference as a result of advances in the field of fluid regenerative actuation that is motivated by widespread use of robotics and mobile machines [22],[23]. The paper exploits the full controllability of a fixed-speed pump drive by utilizing star/delta starter and fluid (hydrodynamic) coupling. Since the efficiency of variable-speed fluid coupling as well as the driving motor decreases as the slip speed between the motor shaft and pump shaft increases, their combined rated efficiency is exploited here using hysteresis liquid-level control to fully load/no-load the motor driving pump (i.e., clutch mode) where the regenerative actuation can easily be implemented [23]. Besides, three motor states, during inflow off period, are distinguished and named analog to the computer's ESMs. A logic algorithm is constructed to select the best motor state for energetic cost reduction considering motor thermal information and grid-combatable tariff structure. These have the potential to provide safe motor operation and alleviate power quality concern. Since there is no fast inrush starting currents, the supervisory control operates the switched VAR compensator (having one third of the normal motor starting VAR consumption) simultaneously with the motor starting using simple delay compensation control and electromechanical contactors. Hence, the system can comply with the connection requirements of μ-grids having limited VAR support and avoid high penalty on voltage dips. In order to obtain highly reliable and smart star/delta starter, a current-based digital method is synthesized here for the contactor life-cycle counting, primarily interlock, and malfunction alarming. An improved FL availability assessment is designed for the starter to be deployed on cloud computing with machine learning. This has the potential to provide pre-fault tolerance for the contactor and preventive maintenance service at low cost. Furthermore, RNN-based full state estimator is developed along with Wald's likelihood ratio test in order to provide post-fault tolerance for the feedback control against sensor defects.

In the following sections, the controlled drive system will be introduced. In Section II, RNN based hysteresis liquid-level controller is presented with supervision capability to detect and tolerate sensor defects. In Section III, the IM drive is described and a closed-transition star/delta starter has been adopted considering techno-economic reasons. Three-states for the motor connection at no load have been identified and named analog to the popularly used computer's ESMs. The problems associated with the motor on/off operation are alleviated, in Section IV, by designing a logic algorithm which selects the least expensive motor state at no-load. Section V introduces a smart electrical health prediction system to manage preventive maintenance for the star/delta starter using current based life-cycle counting, interlocking, and malfunction detection method. Cost analysis and efficiency study, using time-based cascaded energy-conservative systems describing the main motor operation, are carried out on IM test ring. The results are introduced and discussed in Section VI. The conclusion is outlined in Section VII.

II. RNN-Based Supervisory Controller

A. Hysteresis Liquid-Level Control

Hysteresis liquid level control is based on direct pumping of liquid such that its level or head h approximates its reference value h^* in average sense. The hysteresis block in Fig. 2 (a) compares the difference between h^* and h with a defined band, Δ, as follows

$$\begin{cases} 1 & h^* - h > \Delta \\ nochange & -\Delta < h^* - h < \Delta \\ 0 & h^* - h < -\Delta \end{cases} \quad (2)$$

The pump on-off operation depends on whether the measured head reaches the upper or lower value of the hysteresis band. Fig. 2 (b) demonstrates an example for the liquid level and input pump flow at steady state. The variation of hysteretic control period ($T = T_{on}+T_{off}$) due to operating point changes can be predicted, compensated, and synchronized with the optimization period by using a fully digital technique and variable hysteresis band as in [6].

B. RNN-Based State Estimator

For fault-tolerant capability, the measured head h is replaced by its estimate value $\tilde{h}$ in the feedback control loop. The problem of pure integrator windup in (1) is cured by proposing full-state estimator based on feed-forward neural network with recurrent architecture (i.e., RNN) as shown in Fig. 3. The RNN has one input layer, one hidden layer, one output layer, and biasing source. The input and output layer neurons are dictated by the number of respective signals and the hidden layer neurons with sigmoid activation function. Since the number of input neurons exceeds what is necessary to determine the output pattern, i.e. over-determined or redundant NN, it can work after training with one (or two) of its input neurons inhabited. This is similar to the case if one (or two) of the plant sensors is defected.

The fault-tolerant ability of the proposed RNN state estimator has the potential to improve the overall availability of the sensing elements. To demonstrate this, we assume that

q_o, q_i, and h sensors have availability A of 80% each. The resultant availability of a RNN estimator, trained with one out of three sensors defected, will be $[1-(1-A_1A_2)(1-A_3A_2)(1-A_1A_3)] = 1-0.36*0.36*0.36 = 95.3344$ %. Furthermore, if the load flow q_o is dependent variable or its profile is known, the RNN can be trained as a best fit estimator with two sensors defected, i.e., of two out of three sensors, which increases the overall availability to $[1-(1-A_1)(1-A_2)(1-A_3)] = 1-0.2*0.2*0.2 = 99.2$ %. Here, we assume that the availability of microprocessor-based data acquisition card = 100% and the availability A=1-failure rate.

The RNN training data comprise q_o, q_i, and h measurements as the input and also as the desired output pattern while, their corresponding estimates are the RNN output pattern. We consider that the network is being trained by the input pattern n, the weights and biases of the network are updated using the back-propagation technique to minimize the network performance function. A common performance function for the feed-forward networks is the mean squared error, MSE:

$$MSE = \frac{1}{Q}\sum_{k=1}^{Q}(d_k^n - \widetilde{y_k^n})^2 \quad (3)$$

where $\widetilde{y_k^n}$ = output of the k^{th} neuron in the output layer, d_k^n the corresponding desired output, and Q = dimension of the output vector (in our case Q = 3). The weights of the neurons are altered to minimize the value of MSE by gradient descent method [10], [14].

C. Sensor Fault Detection and Discrimination

For RNN training, measurement sets of tank variables shall be collected online during periodic phases of data acquisition. An averaged signal for each channel is computed and considered as a reference pattern. Cross correlation between coefficients of single samples and the averaged pattern are calculated. The samples with very low correlation coefficients are discarded. Fig. 4 (a) demonstrates simulated time response (using MATLAB/Simulink) of RNN based estimator for the pump outflow during training, testing, and validation phases using input signal with white noise. Fig. 4 (b) shows the samples autocorrelation-error curve and the corresponding level of confidence.

The confidence limit is similarly determined for sensor fault detection using Wald's likelihood ratio test. The method is based on choosing between two hypothesis H_0 (normal behavior) and H_1 (abnormal behavior) according to signal signature [24]. For each error signal E_k(t), we define $P(E_k^J/H_o)$ and $P(E_k^J/H_1)$ as a priori density probability where E_k^J is a vector of J samples of the signal E_k(t). The likelihood ratio is given by

$$\gamma_k = \frac{P(E_k^J/H_o)}{P(E_k^J/H_1)} = \prod_{i=1}^{J}\frac{P(E_k^i/H_o)}{P(E_k^i/H_1)} \quad (4)$$

Then the formulation of Wald's test is given by (5):

$$\begin{cases} normal & A > \gamma_k \\ no\ decision & A < \gamma_k < B \\ abnormal & B < \gamma_k \end{cases} \quad (5)$$

where A = $P_{MF}/(1-P_{RA})$ and B = $(1-P_{MF})/P_{RA}$ with P_{MF} is the probability to miss faulty measurement and P_{RA} is the probability of wrong alarm.

Wald's test for sensor fault detection can be formulated in terms of significant deviation of the reference mean value μ assuming, $P(E_k^J/H_o)$ and $P(E_k^J/H_1)$ are Gaussian:

$$\begin{cases} normal & \sum_{i=1}^{J} V_i < T_o \\ no\ decision & T_o < \sum_{i=1}^{J} V_i < T_1 \\ abnormal & \sum_{i=1}^{J} V_i > T_1 \end{cases} \quad (6)$$

The two test frontiers are as in (7):

$$T_0 = \frac{\sigma^2 lnA}{\mu_0-\mu_1} \& T_1 = \frac{\sigma^2 lnB}{\mu_0-\mu_1} \quad (7)$$

and

$$V_i = E_i - \frac{J(\mu_0-\mu_1)}{2} \quad (8)$$

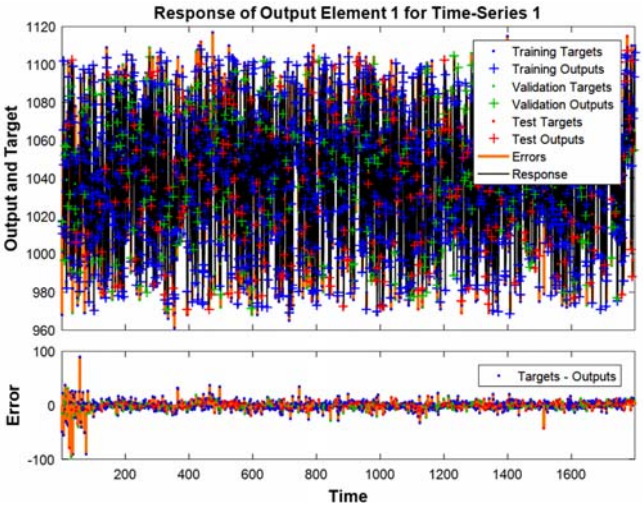

Fig. 4 (a) Time response of the RNN

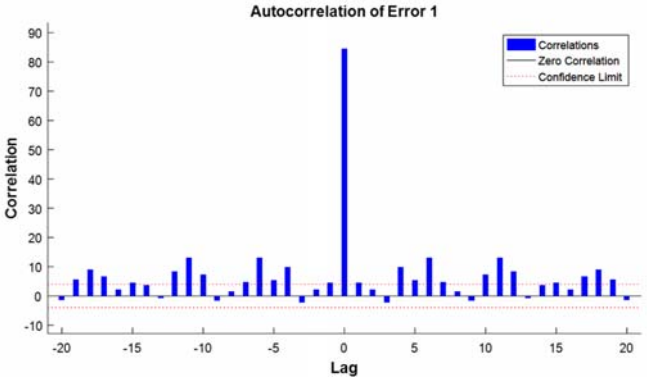

Fig. 4 (b) Autocorrelation-error curve

Here, we assume that the mean value μ_o and the variance σ^2

are determined during learning phase using sensor data-sheet and μ_1 is the increase (or decrease) in μ checking in which the sensor fault detector will be triggered as illustrated on Fig. 5 (a). Consequently, the output of Wald's test will inhabit the defected sensor signal and the corresponding input neuron will be assigned to its delayed estimate signal as depicted schematically in Fig. 5 (b). Further, Wald's test can be repeated more than once (analog to the automatic circuit recloser operational sequence) in order to discriminate between temporary/transient and permanent sensor failures. In case of wireless sensor network (WSN), modeling of WSN under transient failures can be given by the manufacture or developed through simulation and experimentation [25], [26].

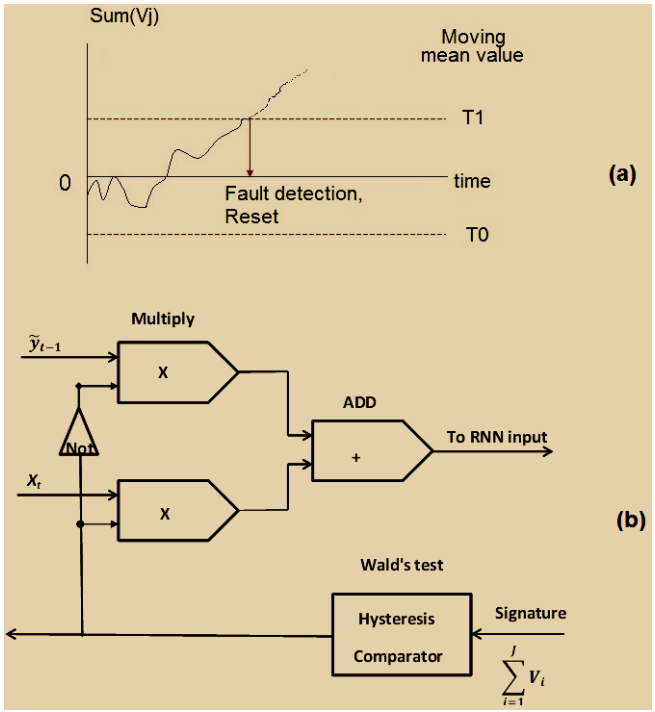

Fig. 5 Mean value, boundaries, and sensor fault detection (a) and schematic diagram of defected signal replacement (b)

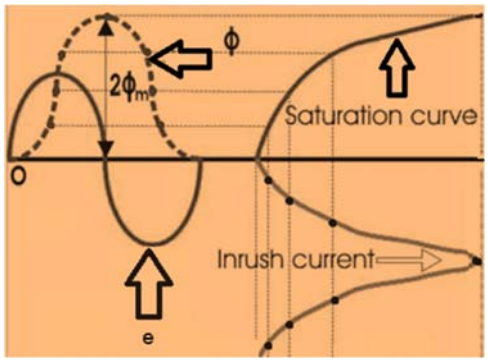

Fig. 6 Inrush current due to core saturation

III. Main IM Drive

A. Closed-Transition Star/Delta Starter

In application such as pumped storage, the energy conservation principle and components efficiency, rather than the pump affinity law, determine the energy savings. Therefore, dynamically varying the pump speed is less important than the pump starting, stopping, and drive train isolation. In such a case, the combination of electromechanical star/delta starter with a fluid clutch, as shown in Fig. 1, represents a good fit. Such a drive is controllable and enable the motor to be rated on running rather than starting torque and experiences lower thermal stress than on/off motor control [19], [27].

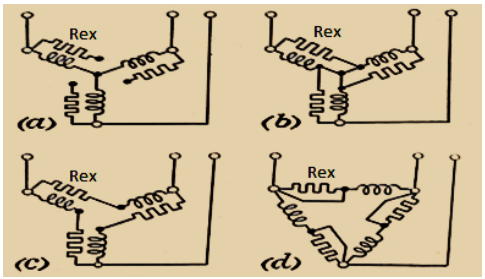

Fig. 7 Closed-transition sequence of operation [27]

The motor starts at no load with star connected stator windings, reducing the starting current and torque to one third of their nominal values. When the motor speed approaches the synchronous speed ω_1, the stator connection is changed to delta. Then, the fluid coupler gradually starts to load the motor by gradual coupling of the pump shaft to motor shaft. Mechanical clutches that operate too early or too suddenly will also produce severe current peaks or catastrophic pressures in the pipelines and motor shaft [14]. But current surges may occur for another reason even when care is taken to avoid premature operation of a change over switch. In fact, any starting method that involves a momentary disconnection of the supply main (such as; autotransformer and star/delta switch) may cause transient current surges of a very severe nature due to remaining voltages across its terminals that decay gradually with a rate depends on the rotor open circuit time constant in the temporarily open circuited stator windings. When the star switch now closes in delta position, the supply voltages are reconnected to stator windings that have induced emfs of comparable size but with a relative time shift that may be anything between coincidence and opposition. In the former case, there will be a very large current surge in all phases and possibly reinforced by the magnetic saturation effect.

Accordingly, by considering negligible speed drop at no load and waiting till the remaining voltages nearly vanish and then closing the star switch in the delta position will not guarantee safe starting because of core saturation. In such a case, high inrush current may flow if the switching occurs while voltage passes near zero due to doubling of the magnetic flux (φ) as illustrated graphically in Fig. 6. This inrush current will last many line frequency cycles, due to high rotor impedance at no load speed, and its energy could be sufficient to trip the circuit breaker, CB shown in Fig. 1, or causing severe voltage dip. To avoid these current surges, a star/delta

starter with closed-transition is adopted here to maintain the connection between stator and supply line, by inserting an external resistance, while changeover is made [27]. The star to delta closed-transition sequence of operation is shown in Fig. 7. The motor is switched on in star (a), resistors are paralleled with the phases (b) leaving the motor itself unaffected; the motor star point is opened (c) putting the windings in delta with series resistance; and (d) the resistors are short-circuited. The method is limited to normally delta connected motors up to rated voltage of 3000 V since, high voltage motors are usually star connected for techno-economic reasons.

B. Three-State ESM

By considering the controllability of the main drive, three possible states for the motor during inflow off period (T_{off}) can be discriminated. They are named, analog to the popularly used computer's ESMs as follows [15], [27]:

1. Sleeping Mode

The motor is decoupled from the pump shaft and runs at no load with delta connected stator windings. The active and reactive energy consumptions, $W_{nl\Delta}$ and $Q_{nl\Delta}$ respectively, are given by

$$W_{nl\Delta} \approx \frac{3V_1^2}{R_c} T_{off} \,\&\, Q_{nl\Delta} \approx \frac{3V_1^2}{X_m} T_{off} \qquad (9)$$

where V_1, R_c and X_m, respectively, are the per phase nominal voltage, no load resistance and, magnetizing reactance. Thanks to the fluid clutch, this mode of operation achieves remarkable energy savings compared with preventing the pump flow using throttling valve.

2. Hibernate Mode

The motor runs at no load with its terminals star connected. The energy consumptions, W_{nlY} and Q_{nlY} respectively, will be reduced to one third of (9) assuming linear magnetic circuit, i.e.,

$$W_{nlY} \approx \frac{3(V_1/\sqrt{3})^2}{R_c} T_{off} \& Q_{nlY} \approx \frac{3(V_1/\sqrt{3})^2}{X_m} T_{off} \qquad (10)$$

However, the motor-pump system in this mode takes relatively longer time to re-operate at full load than the sleeping mode.

3. Shutdown Mode

The motor is disconnected from the grid supply and consumes no active and reactive power. However, it loses the kinetic energy $\frac{1}{2}J\omega_1^2$ stored in its moment of inertia J. For restarting, the motor will dissipate amount of energy equals $\frac{1}{2}J\omega_1^2$ as a heat in the rotor resistance r_2 and $(\frac{r_1}{r_2})\frac{1}{2}J\omega_1^2$ as a heat in the stator resistance r_1 (see the Appendix A). Assuming $r_1 = r_2$, the total active and reactive energy consumptions associated with the shutdown decision, W_{sh} and Q_{sh} respectively, are

$$W_{Sh} \approx 1.5J\omega_1^2 \;\; \& \;\; Q_{sh} \approx W_{Sh} tan(\varphi_{st}) \qquad (11)$$

where, φ_{st} is the motor phase angle at starting. Here, we assume that the reactive energy in (kVARh) is measured by measuring the active energy (kWh) and its power factor [15].

IV. ESM Logic Algorithm

A logic algorithm is synthesized to select the least expensive motor state during inflow off period (T_{off}) considering the motor thermal information and grid-compatible tariff structure (see Appendix B). This is critically important in the event of repetitive overload (starting) where, missing the motor thermal information could lead to numerous problems such as insulation failure. On the other hand, imposing the maximum permissible number of consecutive start/hr as a constraint in the water network optimization problem adds difficulty. In the followings, a logic flowchart that can relax this burden will be presented based on the following assumptions:

(i) The fluid clutch uses regenerative actuating method such that its energy loss can be neglected [22].
(ii) The variation of hysteresis control period ($T=T_{on}+T_{off}$) with the operating point changes can be compensated [6].

The algorithm's flowchart is shown in Fig. 8 and described in Table I where, θ and τ are the temperature-rise (above ambient) and thermal time constant, respectively (see Appendix A).

TABLE I
DESCRIPTION OF THE LOGIC FLOWCHART OF FIG. 8

Step	Description
1	Read the data base file. The following data must be supplied; motor thermal rates, cost of 1 kWh, cost of 1 kVARh and any power quality (PQ) indices if existing, no-load active and reactive losses.
2	Input the motor temperature θ and T_{off} period.
3	Calculate the costs of motor being delta or star connected during T_{off} from (9) and (10), cost of shutdown from (11), and any existing PQ index term, the depreciation cost of star/delta starter. The depreciation cost is calculated based on the gross cost of star/delta starter divided by its expected number of switching operations before failure; typically (500,000-1000,0000 times) or (250,000-500,000 life cycles).
4	If the star connection cost is greater than shutdown cost, go to step8.
5	If the cost difference between delta and star connections is less than or equal to the depreciation cost, go to step7.
6	Change the motor connection to star (hibernate mode).
7	Keep the motor delta connected (sleeping mode).
8	If θ is greater than θ_{safe} go to step10. The safe temperature θ_{safe} is calculated using starting current ratio and the acceleration time.
9	Shutdown mode.
10	Calculate the time (t) needed to reach θ_{safe} from (17).
11	If (t) is less than (T_{off}) go to step12else go to step5.
12	Wait time (t) to cool the motor to θ_{safe}.
13	Update the cost functions in terms of (T_{off}-t).
14	Go to step4.

V. Smart Starter Electrical Health Assessment

Automatic star/delta switch comprises electromagnetically actuated 3-phase contactors that change the motor connection in cyclic making and breaking operations. This results in inevitable wear and tear and impacts the electrical health of the contactor. Since highly reliable contactors are required, studies have been carried out in order to predict the contactor

failure by monitoring its operational parameters [17], [18]. In [18], a sample-data based ANN model is developed to estimate the remaining life-cycles utilizing the monitored contact resistance. However, the method is expensive since very accurate measurements of the contactor voltage and current are required. In order to overcome this problem, we adopted using the inverse model of [18], i.e., the contact resistance as a function of the contactor (on-off) switching-cycles [15].

A simplified piecewise linearized model has been used as shown in Fig. 9. The trend of the resistance variation changes with the number of switching-cycles. Accordingly, the contact resistance can be evaluated at low cost. Unlike [15], the digital counter proposed here is based on current sensing, as shown in Fig. 10 for the a-phase current i_a, which is also needed for the digital thermal protection. Therefore, no additional sensor cost is required. The routine to assign the gating signal of the a-phase delta contactor S_{Da} to its command, in the proposed algorithm, is shown in Fig. 10 and explained in Table II.

TABLE II
DESCRIPTION OF THE LOGIC FLOWCHART OF FIG.10

Step No.	Description
1	Sample i_a current using Analog/Digital converter.
2	Calculate the current r.m.s value $I_{rms}^2 = \frac{1}{n}\sum_{k=1}^{n} i^2$ (k).
3	If I_{rms} equals to zero-threshold go to step4 else go to step6.
4	If the gating signal of a-phase star contactor S_{Ya} is high go to step10.
5	Set the Enable line of the a-phase delta contactor to 1 and the Disable line to 0, go to step8.
6	If the gating signal of the a-phase star contactor S_{Ya} is low go to step10.
7	Set disable line of a-phase delta contactor to 1 and the Enable line to 0.
8	Assign the gating signal of a-phase delta contactor S_{Da} to its command and wait proper delay for executing the closed-transition.
9	Calculate the switching count from its previous value and Enable and Disable values, go to other routines.
10	Set malfunction alarm for inspection after checking delta position status.

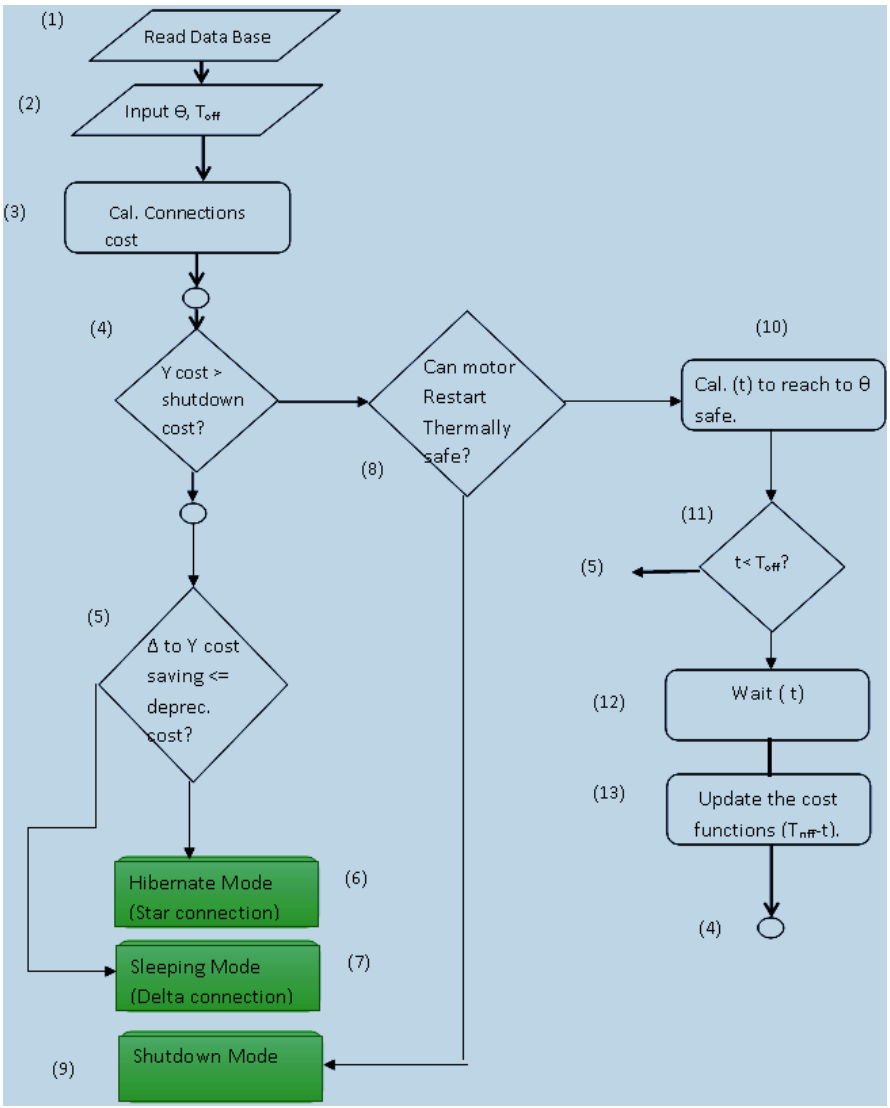

Fig. 8 Three-state ESM Logic selector

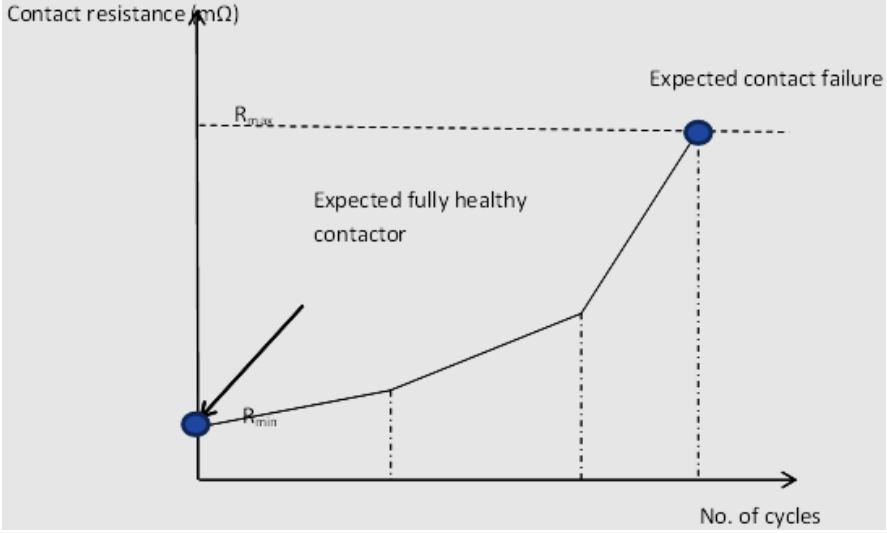

Fig. 9 Contact resistance variations with the life-cycles

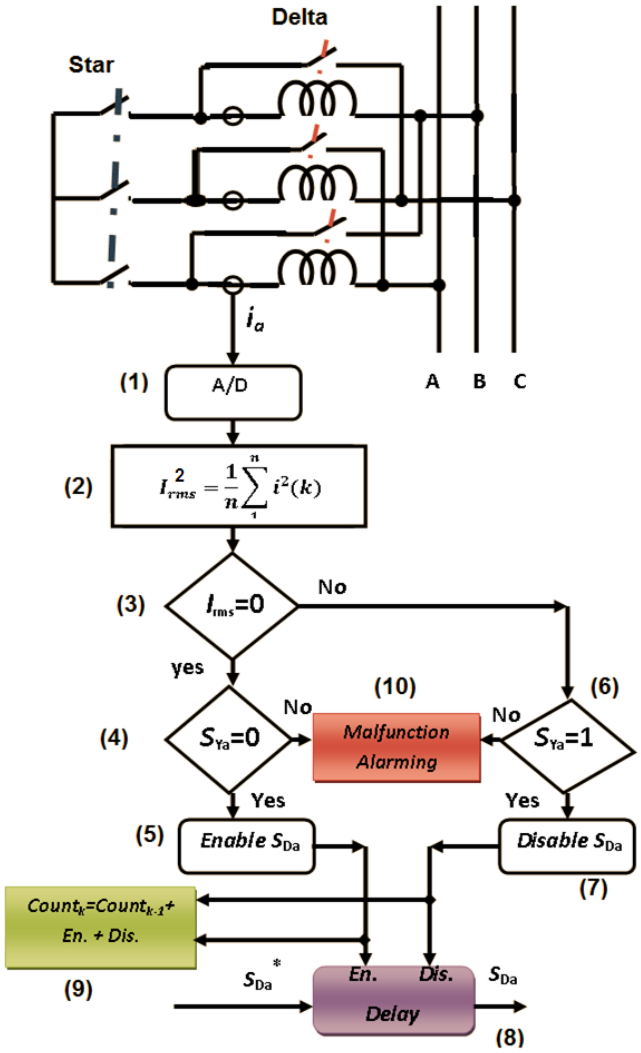

Fig. 10 Digital counter, interlocking, and malfunction detection

The routine to assign the gating signal of the a-phase star contactor, S_{Ya}, to its command is obtained by interchanging S_{Ya} and S_{Da} in blocks (4) to (10) in Fig. 10. The procedure for b and c phases are straightforward similar and in case of 3-phase contactor we have; $S_{Ya,b,c} = S_Y$ and $S_{Da,b,c} = S_D$. The algorithm services as a counter for the contactor's operational life-cycles, preliminary interlocking, and malfunction alarming. These features, in addition to estimation of the remaining life-span of star/delta switch, have the potential to provide smart starter with highly reliable operation.

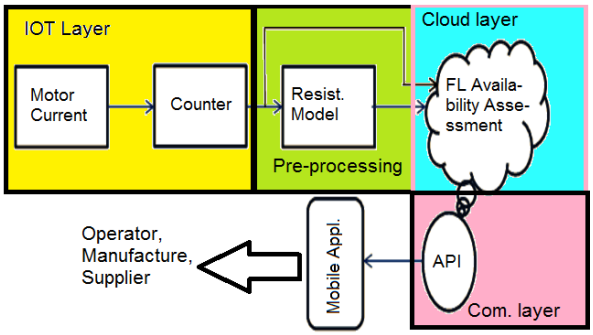

Fig. 11 Starter health prediction system: Information flow

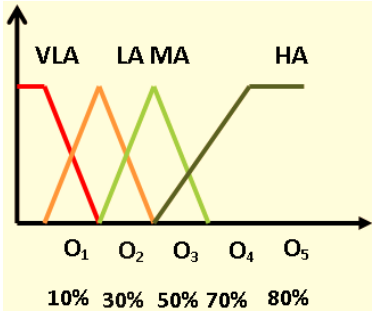

Fig. 12 Output membership function

Compared to [15], an improved availability assessment is designed here using FL computing to evaluate the electrical health of the starter. The FL computing has the advantage to

handle such multi-valued, nonlinear, and probabilistic knowledge with more accuracy [28]. The information flow of the proposed smart availability assessment is shown in Fig. 11. The system composed of layers such as; data collection layer, data preprocessing layer, availability assessment or starter health prediction layer, and communication layer. The FL algorithm is deployed in the cloud layer and has two inputs and one output. The output membership is demonstrated in Fig. 12 with initial parameters settings where HA, MA, LA, and VLA stand for high, medium, low, and very low availability, respectively while the FL rules are demonstrated in Table III. The parameters ($O_{1..5}$) of the fuzzy membership function can be adjusted on cloud with a reference to the manufacture's reliability database and enclosure ingress protection (IP) code. The communication layer sends warning messages to the operator, manufacture, and supplier in case of low starter availability as well as a prediction for the remaining life-span. This has the potential to interactively manage a preventive maintenance for the starter and reduce the risk factor of wear and tear, and downtime [29].

TABLE III
FL RULES

Contact resistance / Life cycles	Small life cycles	Medium life cycles	Large life cycles	Very large life cycles
Large Resistance	MA	MA	LA	VLA
Medium Resistance	HA	MA	MA	LA
Small Resistance	HA	HA	MA	LA

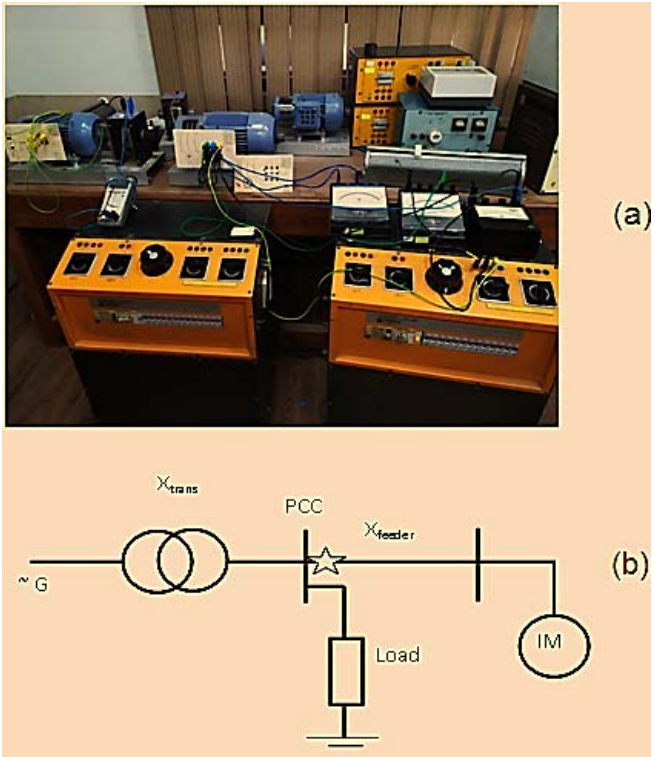

Fig. 13 IM Testing setup (a) and radial distribution system feeding the motor with a marked location for PFC (b)

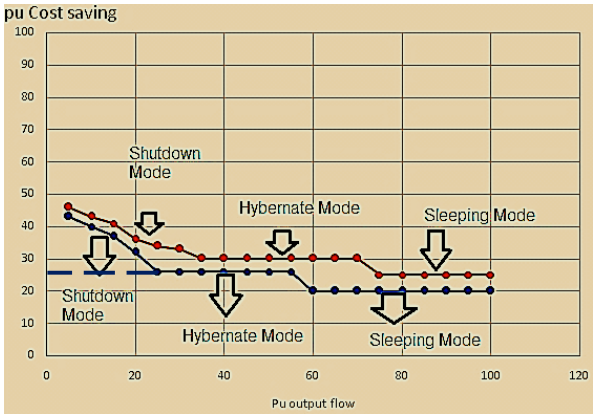

Fig. 14 Percent cost saving as a function of the % output flow

VI. Cost and Efficiency Studies

Preliminary testing has been carried out on a 3-phase, 50 Hz, 4-poles, 240 V, delta-connected IM using a laboratory setup shown in Fig. 13 (a). The objective of the tests is to determine the various motor characteristics required for the logic flow ESM selector (such as; no load active and reactive power losses, per unit starting current, rotor and stator resistances, moment of inertia, motor thermal rates...etc.) considering the following conditions: ambient temp. Θ_{amb} = 30 °C, Trip temp. Θ_{Trip} = 90 °C (Y class of insulation), and safe temp. for restarting Θ_{safe} = 70 °C. Furthermore, a radial distribution system as shown in Fig. 13 (b) is assumed to supply the motor and emulated in the Lab where the reactance of the transformer and motor feeder is 4.3%, starting current = 3.2 pu, and acceleration time ≈ 4 s. The voltage dip at the point of common coupling (PCC) is considered as a sudden reduction of the rms voltage followed by recovery after a period of time from half cycle to one minute over 10% and less than 100% [31], [32]. Here, we put a PQ penalty of 1% pu cost for each voltage dip occurrence due to motor shutdown and restarting that is over 10% and less than 20%.

A per unit cost analysis is performed assuming that the following parameters; C_e = 1 pu, C_Q = 0.4, and T = 30 min, respectively, are the cost of 1 kWh, cost of 1 kVARh, and the optimization control period. The parameter C_Q is set greater than the cost of reactive power device needed for compensation (see Table IV). The cost analysis results are shown in Fig. 14, in percent at constant head, with and without fixed VAR compensator installed at the upstream feeder end as a power factor correction (PFC) method, respectively, indicated by the red and blue curve. The relative cost savings are calculated with respect to the throttling cost.

The throttling power losses are emulated in the Lab. as a brake during the temperature-rise test which is carried out using two identical IMs connected to the same shaft. The first motor (the driving one) runs at rated positive sequence voltages while the second motor is supplied by reduced negative sequence voltages and rotates as a brake against its rotating field. In that test, the temperature-rise curves of the driven motor (brake) are determined, as well as; the throttling power losses are approximated to the input powers to the

driving machine. Fig. 14 depicts noticeable effects of delta/ star transition on pu cost savings at medium flow rates. The reduction of cost savings by using restrictive tariff structure (blue curve) can be justified, from the utility point of view, by limiting the electric voltage disturbances due to repetitive starting and as a motivation for using reactive power compensation method (red curve) [12], [27], [30].

In case of μ-grids with limited VAR support or remote locations with high penalty on voltage sags due to motor starting, the shutdown mode will disappear and hibernate mode will be extended to the low flow region. The cost difference indicates that more energetic cost reduction at low-flow rates can be achieved by either: (a) using an auxiliary VSI-fed IM pumping unit with efficiency optimized speed control at low flow rates [14] or (b) using a low-rated (one third of the normal starting VAR) switched VAR compensator to start/shutdown the main motor economically. Since, the voltage sag at the PCC would decrease from about 14% to less than 7%. Thanks to the closed-transition star/delta starter, this solution can easily be realized using electromechanical contactors with simple delay compensation control.

Here, we adopt using the two solutions to ensure flexible 30% of the system throughput in case of main motor/pump failure or μ-grid operating in the stand-alone mode. In addition, employing the two solutions could increase the system efficiency and hence revenue because the auxiliary machine will have higher pu loading at low flow rates than the main unit due to base rating difference. As well, the cost of VSI decreases sharply at small power ratings.

For comparison, typical costs of the main components of the proposed drive system and a DFIM are estimated from three different suppliers on the internet. Table IV depicts the results where; the base X is the cost of a fully-rated squirrel cage motor/pump. The DFIM is assumed to be able to operate over wide speed control range. The machine operates as a single fed IM at low speed range and as a DFIM at medium and rated speed ranges utilizing star/delta switch for efficiency improvement. The common items between the two systems are removed for clarity whilst the extra cost includes the cost of crowbar protection and synchronization circuits in case of DFIM and represents an additional installation cost for the proposed drive. The results indicate that the presented drive system is more expensive than DFIM by about 3% which is marginal. A comparison between the operations of DFIM and the proposed drive system will explicitly lead to higher efficiency for the latter one due to lower power electronic converter losses and rating of the auxiliary machine.

TABLE IV
COST COMPARISON BETWEEN PROPOSED DRIVE SYSTEM AND DFIM

Component cost / System	Motor & Pump	30% VSI	VAR Compensators	Extra-cost
Proposed Drive	Squirrel Cage (2X+0.6X)	Single (0.5X)	(X/3)	0.3X
DFIM	Wound rotor (1.5X+X)	Dual (X)	-	0.2X
Cost Difference	0.1X	-0.5X/	X/3	0.1X

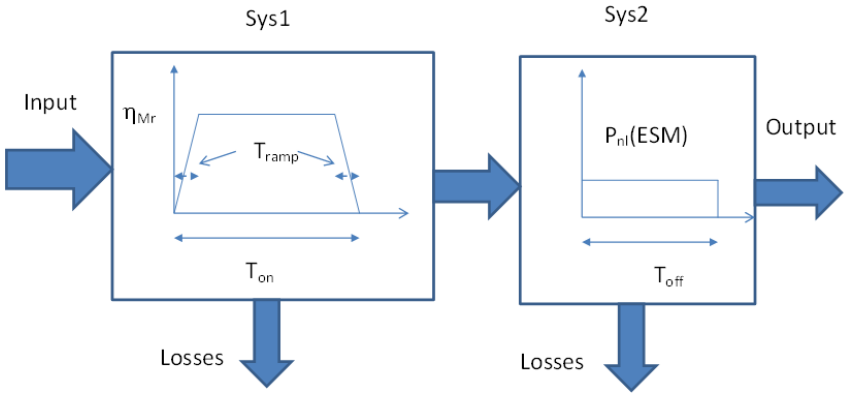

Fig. 15 Timely-Cascaded systems for efficiency evaluation

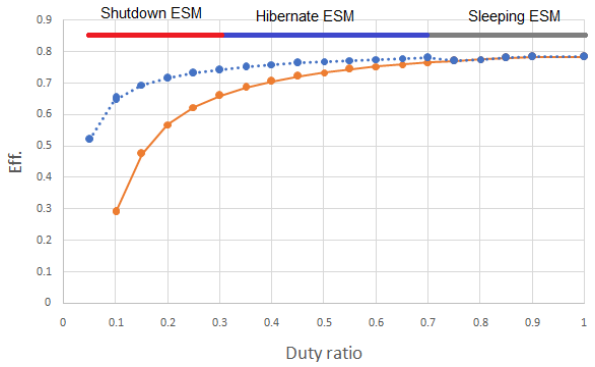

Fig. 16 Estimated motor efficiency with (dashed line) and without (solid line) ESMs

For efficiency evaluation, the principle of energy conservation is applied to the main drive. The T_{on} and T_{off} control periods are represented by two timely-cascaded systems Sys1 and Sys2, respectively, as depicted in Fig. 15. In Sys1, the motor efficiency is considered to vary linearly during the ramp time T_{ramp} and constant at its rated value η_{Mr} otherwise. The efficiency of Sys1 averaged over T_{on} is given by (12) where the duty ratio $D = T_{on}/T$ and $T = T_{on} + T_{off}$:

$$\eta_{on} = \eta_{Mr}\left(1 - \frac{T_{ramp}}{DT}\right) \quad (12)$$

The efficiency of Sys2 over T_{off} period is given by (13) where P_{nl} (ESM) is the pu no-load loss as a function of ESM

(see Section III *B*):

$$\eta_{off} = \frac{\eta_{on} - (1-D)P_{nl(ESM)}/D}{\eta_{on}} \quad (13)$$

The combined efficiency is then given by:

$$\eta_{eq} = (\eta_{on}\eta_{off})\eta_{clr} \quad (14)$$

Here, the efficiency of the fluid clutch is assumed to be constant at its rated value η_{clr} as a result of regenerative actuation. Fig. 16 shows the estimated efficiency of the IM, shown in Fig. 13, with (dashed line) and without (solid line) the introduced ESMs assuming: t_{ramp} = 12 s, η_{clr} = 95%, and constant head. The results depict efficiency improvement at medium and low duty ratio (i.e., output flow rates). However, more energy savings could be achieved at low flow rates by employing the low rated; VSI-fed; auxiliary unit. Fig. 17 demonstrates an optimistic expectation where the efficiency of the auxiliary drive is assumed to be equal to that of the main unit with ESMs and a base loading shift. The efficiency increase (gray bars) is 25% maximum and 15% as an average. The actual efficiency improvement could approach the optimistic one provided that the PWM-VSI losses and the machine iron losses are minimized using efficiency optimized inverter module and a flux optimization technique [33], [14]. In [14], it was shown that the excess machine losses due to PWM voltages and harmonic currents have noticeable impact and therefore; were considered in the flux optimization problem using closed form equations since using hard switched IGBT or IGCT modules working at moderate switching frequency and impulse overvoltage protection is the common industry practice to provide economical pump drive at high power rating. This is because most soft-switching techniques, to realize high switching frequency and compact sinusoidal output filter, require extra active components and hence; increased cost. These difficulties were cured in [33], where the inverter output filter is used to achieve current harmonic minimization as well as zero voltage switching. This is especially beneficial in case of distributed generation and machine drive with WSN where; cost, efficiency and electromagnetic compatibility are important design factors.

VII. Conclusion

This paper described an efficient IM drive system having high availability at low cost and control over the whole range for water pumped storage. The paper utilized three-state ESM at no load and logic selector for the main drive with smart star/ delta switch and fluid coupler working in regenerative clutch mode. The procedure implements the motor thermal information and grid compatible tariff structure to reduce energetic cost. Current-based digital method for the contactor's life-cycle counting, primary interlocking, and malfunction detection is presented along with improved contactor electrical health predictor. These have the potential to manage interactive preventive maintenance and provide reliable contactor's operation at low cost. The paper also proposed a hysteresis liquid-level controller with sensor fault tolerance utilizing RNN estimator and Wald's likelihood ratio test for fault detection and discrimination. An auxiliary, efficiency-optimized, VSI-fed drive is proposed to increase the system availability, revenue, and flexibility for green Power-Water networks during islanding with insufficient reserve and high level of uncertainty. Investigations using computer simulations, theoretical analysis, cost and efficiency studies using a laboratory IM setup have been conducted and the results showed the validity and effectiveness of the introduced system and control.

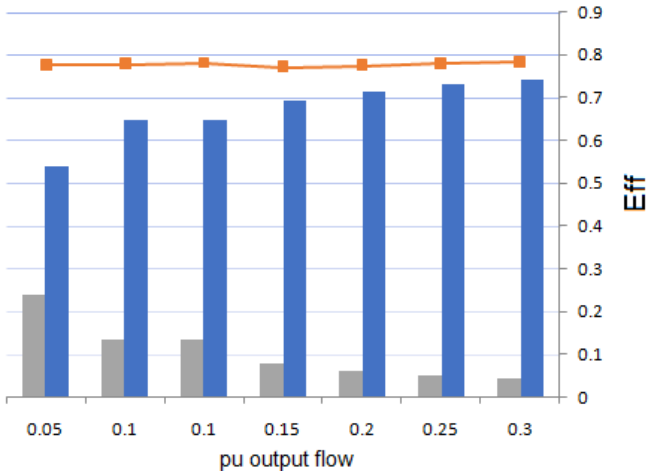

Fig. 17 Estimated efficiency difference (gray bar) between main (blue bar) & auxiliary (orange line) units

Acknowledgment

The authors would like to thank the people who helped them during writing phase of this work and the reviewers for their constructive comments.

Appendix A

Basically, digital thermal overload protection depends on the I^2t principle and is derived from the first order thermal model in (15) [15], [19]:

$$\frac{d\theta}{dt} = \frac{1}{\tau}(\theta_f - \theta) \quad (15)$$

where $\theta, \theta_f,$ and τ, respectively, are temperature-rise (above ambient), final temperature-rise (above ambient), and thermal time constant. The recursive temperature solution to (15) is given in (16):

$$\theta_n = \theta_{n-1} + (\theta_f - \theta_{n-1})(1 - e^{-\frac{\Delta t}{\tau}}) \quad (16)$$

where $\theta_n, \theta_{n-1},$ and Δt, respectively, are the calculated present temperature, temperature at previous time step and time step between calculations. Further, $\theta_f = (I/I_{ref})^2 T_{ref}$ where I, I_{ref}, and T_{ref}, respectively, are the motor phase current, set current reference, and set temperature rise reference. Thermal Capacity Used (TCU) is calculated based on rated

motor current with an overload factor applied and expressed as a percentage of maximum temperature. The thermal protection trips when TCU reaches 100%.

Calculation of the time to reach a specified temperature θ based on load and preload temperature is given by

$$t = \tau \ln\left(\frac{\theta_f - \theta_o}{\theta_f - \theta}\right) \quad (17)$$

REFERENCES

[1] H. B. (Teddy) Pŭttgen, "R&D in our industry: where do you go from here?" *Inter. Conf. on power system technology, Powercon2004, Keynote Address, Singapore, 2004, pp.9-10.*

[2] S.M. Kaviri *et al.*, "A Supervisory Control System for Nano-grids Operating in the Stand-Alone Mode, "*IEEE Trans. on Power Electr., Vol. 36, No. 3, March 2021, pp. 2914–2931.*

[3] N. Mousari et al," A Real time energy management system for pumped hydro storage systems in farmhouses," *ELSEVER, Journal of energy storage, No.32,2020.*

[4] B. D. Brown, J. A. Lopes, and M. A. Matous, "optimization of Pumped Storage Capacity in an Isolated Power System with Large Renewable Penetration," *IEEE Trans. On power systems, Vol. 23, No. 2, 2008, pp. 523-531. DOI:10.1109/TPWRS.2008.919419.*

[5] C. Jin, N. Lu, S. Lu, and Y.V. Makarov, "Coordinated Control Algorithm for Hybrid Energy Storage Systems," DOI:10.1109/PES.2011.6039893,2011.

[6] W. Stefanuti and P. Mattavelli, "Fully Digital Hysteresis Modulation with Switching Time Prediction," *IEEE Trans. On Ind. Appl., Vol. 42, No. 3, 2006 pp.763-769.*

[7] O. S. Ebrahim and P. K. Jain "LQR-based Stator Field Oriented Control for the Induction Motor Drives," *the23rd IEEE Appl. Power Electr. Conf. (APEC 2008), USA, 2008.*

[8] O. S. Ebrahim, M. F. Salem, M. A. Badr, and P. K. Jain," Application of linear quadratic regulator theory to the stator field oriented control of induction motors" *IET Electr. Power Appl., 2010, Vol. 4, Issue 8, pp. 637–646.*

[9] G. C. Goodwin and K. S. Sin, "Adaptive Filtering Prediction and Control," *Dover Publications, New York, 2009.*

[10] F. M. Salem, "Recurrent Neural Networks: From Simple to Gated Architectures," *Springer publications, 2022.*

[11] The European commission efficiency regulations (EU) 2019/1781:For low voltage electric motors and variable speed drives, 2019.

[12] A. David, J. Maire, and M. Dessoude, "Influence of voltage dips and sags characteristics on electrical machines and drives," *the 3rd inter. Conf. on power quality end user Appl., PQA94, Netherlands, 1994, No. 1B-1.31.*

[13] Jardic*et al*, "Method and Apparatus Detecting a Failed Thyristor," *Patent No. US 6,211,792 B1, 2001.*

[14] O. S. Ebrahim, A. S. Elgendy, M. A. Badr, and P. K. Jain," ANN-Based Optimal Energy Control of Induction Motor in Pumping Applications," *IEEE Trans. on Energy Conversion, no.3.1, Oct. 2010.*

[15] O. S. Ebrahim, K. O. Shawky, M. A. Badr, and P. K. Jain "Supervisory Control for Induction Machine with a Modified Star/Delta Switch in Fluid Transportation," *World Academy of Science, Engineering and Technology Inter. Journal of Electrical and Computer Eng., Vol.16, No.12*, 2022.

[16] I. Miller, "Fluid Couplings vs VFDs for High Inertia Rotating Driven Loads: A Selection Guide Reviewing the Merits of Both Options, "*Power Transmission Engineering, pp.44-46, 2017.*

[17] S. Kumari *et al*, "Reliability Estimation of Distribution Components-Contactors," *IEEE PES Asia Pacific power and Energy Conf., 2016.*

[18] S. Abirami *et al*," AC Contactor Electrical Health Estimator Model, "*IOP Materials Science and Engineering, 2021.*

[19] K. Smith and S. Jain, "The Necessity and Challenges of Modeling and Coordinating Microprocessor Based Thermal Overload Functions for Device protection," *The 70 Ann. Conf. On Protective Relay Engineers (CPRE), 2017.*

[20] B. T. Gorman, " Contingency Analysis for Coupled Power-Water Networks, " Ph. D. thesis, ARIZONA STATE UNIVERSITY, 2020.

[21] W. Leonhard, "Control of Electrical Drives," *2nd Ed. Springer" 1996.*

[22] D. Margolis, "Energy Regenerative Actuator for Motion Control with Application to Fluid Power Systems," Journal of Dynamic Systems Measurement and Control, ASME, 2005. DOI:10.1115/1.1870038

[23] K. Suzumori, New Robotics Pioneered by Fluid Power, Journal of Robotics and Mechatronics, *Special Issue on Fluid Powered System and its Application, Vol.32, No. 5, pp.854-862, 2020.*

[24] A. Wald, "Sequential analysis", *Dover Publications, New York, 1947.*

[25] D. Li, Y. Wang, J. Wang , C. Wang , Y. Duan, " Recent advances in sensor fault diagnosis : A review, " *ELSEVER Journal on Physical Sensors and Actuators, Vol.309, No.1, 2020, doi.org/10.1016/j.sna.2020.111990.*

[26] A. Masoum; A. H. Jahangir; and Z. Taghikhaki, "Survivability Analysis of Wireless Sensor Network with Transient Faults," *IEEE Conf. on Computational Intelligence for Modeling Control & Automation, 2008. DOI: 10.1109/CIMCA.2008.195.*

[27] M. G. Say, "Alternating Current Machines", *John Wiley & Sons, 5th edition, 1968.*

[28] C. Earl, "The Fuzzy Systems Handbook," *1994.*

[29] R. Malhotra; E. McLeod, and T. Alzahawi, "Management and Maintenance of Electrical Equipment in Industrial Facilities: Procedures for Improving Safety While Saving Money, " *IEEE Ind. Appl. Magazine*, Vol. 27, No. 1, pp. 48-54, 2020. DOI: 10.1109/MIAS.2020.3024486

[30] O. S. Ebrahim; P. K. Jain; G. Nishith, "Digital State Control with Preview for a Shunt Active Filter Having the Function of Active Rectifier", *The 33rd Ann. Conf. of the IEEE Ind. Electr. Society* (IECON'07), 2007, Taiwan.

[31] The institute of electrical and electronics engineering (IEEE) publisher, "1346-1998 Recommended Practice for Evaluating Electric Power System Compatibility with Electronic Process Equipment," 1998, DOI: 10.1109/IEEESTD.1998.87816.

[32] H. El. D. Talaat, "Discrimination and Assessment of Voltage Sag in Distribution Networks," *the 23rd inter. Conf. on electricity distribution, CERD, Lyon, 2015.*

[33] S. Eren, M. Pahlevani, S. Pan and P.K. Jain, "High Efficiency Inverter for Distributed Generation," *US Patent No. 9,935,562, April 3, 2018.*

Osama S. Ebrahim received his BSc (Hons), MSc, and PhD degrees from Ain Shams University, Egypt, in 1993, 1998 and 2004 respectively. Since 2005, he has been Assistant Professor in the Electrical Power and Machines Department, Ain Shams University, and has served as a consultant engineer for the Electrical and Mechanical Research Institute, National Water Research Center, Egypt, where he provides scientific guidance in developing energy efficient and environmentally friendly variable speed pumping units. He has pursued research activities as a postdoctoral fellow at the Centre for Energy and Power Electronics Research (ePOWER), Queen's University, Canada, in 2006 and since 2008, with grant funding from the Ontario Ministry of Research and Innovation. Dr. Ebrahim is a member of IEEE and of the Egyptian Syndicate of Engineering. He was a Treasurer of the IEEE Kingston Section, Canada. His research interests include modern control theories and their digital applications to power electronic converters, FACT/s applications to power systems, sensorless motor drives, wind alternators and solar PV systems. Since 2011, Dr. O. S. Ebrahim was with the Faculty of Engineering, Ain Shams University, Egypt, continuing his research work in the area of high performance, efficient and, low cost electrical machine drives and energy systems.

Kareem O. Shawky is a student at the Civil Dept., Faculty of Engineering, Ain Shams University, Egypt. His research interest includes smart cities, building and hydro storage systems and networks, traffic management and control and intelligent cloud computing.

Mohamed A. Badr received the BSc (Hons.) degree from Cairo University, Egypt, MSc degree from Ain-Shams University, Egypt, MASc and PhD degrees from University of Saskatchewan, Canada in 1965, 1969, 1971,

and 1974, respectively. He is a Professor in the Electrical Power and Machines Department, Ain-Shams University since 1986. Currently, he is a chairman in the Egyptian Supreme Council for promoting faculty staff members to higher ranks and Dean of Faculty of Engineering and Technology, Future University, Egypt. Since 2020 he became the Vice President of the future university, Egypt. Dr. Badr has a considerable contribution in developing the electrical and environmental engineering in Egypt and Saudi Arabia where he directed many conferences, workshops, consultant units and held various teaching positions.

Dr. Badr is awarded the Egyptian State Encouraging Award in Engineering Sciences in 1997 and nominated for the UNESCO science prize for outstanding contribution to the scientific development of a member state or region. He is also obtained the Egyptian State Award for Scientific Superiority in Engineering Sciences in 2004. His domain of research activities in the electrical power and machine applications includes interdisciplinary varieties and he published more than 150 conference and Journal papers and three scientific books.

Praveen K. Jain (S'86, M'88, SM'91, F'02) received a BE (Hons.) degree from the University of Allahabad, India, and MASc and PhD degrees from the University of Toronto, Canada, in 1980, 1984, and 1987, respectively, all in electrical engineering.

Presently, he is a Professor and Tier-1 Canada Research Chair in Power Electronics at Queen's University in Kingston, Ontario, Canada. He is also the founding Director of the Queen's Centre for Energy and Power Electronics Research (ePOWER).

From 1994 to 2000, Dr. Jain was a Professor at Concordia University, Montreal, Canada, where was engaged in teaching and research in the field of power electronics. Prior to this (1989-1994) he was a Technical Advisor with the Power Group, Nortel Networks, Ottawa, Canada, where he was providing guidance for research and development of advanced power technologies for telecommunications. During 1987-1989, he was with Canadian Astronautics Ltd., Ottawa, Canada, where he played a key role in the design and development of high frequency power conversion equipment for the Space Station Freedom. He was a design engineer and production engineer at Brown Boveri Company and Crompton Greaves Ltd., India, respectively during the period of 1980-1981. He also has considerable consulting experience with the industry including Astec, Ballard, General Electric, Intel and Nortel.

Dr. Jain has attracted over $20M funding to conduct research and establish the state-of-the-art Energy and Power Electronics Applied Research Laboratory (ePEARL) at Queen's University. He has also supervised over 75 research engineers, postdoctoral fellows and graduate students. He has considerable experience in transferring technology from university lab to practical product designs. He secured over $35M venture funding to found CHiL Semiconductor to design and market mixed analog/digital semiconductor chip products. Dr. Jain has published over 375 publications including 40 patents in the area of power electronics. Dr. Jain is a Fellow of the Institute of Electrical and Electronics Engineering (FIEEE), a Fellow of the Engineering Institute of Canada (FEIC) and a Fellow of the Canadian Academy of Engineering (FCAE). He is also the recipient of 2004 Engineering Medal (R&D) of the Professional Engineers of Ontario. He is an Associate Editor of IEEE Transactions on Power Electronics, and KIPE Journal of Power Electronics. Recently, Dr. Jain has been awarded the 2021 IEEE Medal in Power Engineering.